Energy Reports 14 (2025) 4189–4200

Contents lists available at ScienceDirect

Energy Reports

journal homepage: www.elsevier.com/locate/egyr

Research Paper

Sizing of hybrid renewable energy systems using a floriculture-motivated optimization technique

Juan M. Lujano-Rojas *, Rodolfo Dufo-López, Jesús Sergio Artal-Sevil, Eduardo García-Paricio

Department of Electrical Engineering, University of Zaragoza, Calle María de Luna 3, Zaragoza 50018, Spain

ARTICLE INFO

Keywords:
Hybrid renewable energy systems
Orchard algorithm
Genetic algorithm
Modern optimization techniques
Rural electrification

ABSTRACT

Selecting suitable devices for a hybrid renewable energy system is a crucial step in any electrification project. However, the growing number of manufacturers of photovoltaic panels, wind turbines, batteries, and generators has made the sizing process increasingly complex. This paper proposes the use of a recently developed method, the Orchard Algorithm, to address this challenging optimization problem. The effectiveness of this floriculture-motivated algorithm is demonstrated through a hypothetical rural electrification project in Nigeria, yielding a well-performing solution comparable to that obtained using a genetic algorithm—a method widely accepted and employed in various commercial tools. From a cost standpoint, the solution obtained through OA demonstrates a 0.45 % improvement over that produced by the GA implementation. During the optimization process with OA, the search space was extensively explored, resulting in a 10.65 % probability of uncovering an additional local minimum by repeating the optimization process. This outcome provides supporting evidence regarding the optimality of the identified solution.

1. Introduction

Human development in isolated areas necessitates the provision of affordable energy solutions. In this context, the integration of renewable energy sources with storage systems and conventional generation units, such as diesel or gasoline generators, has demonstrated remarkable effectiveness. A hybrid renewable energy system (HRES) broadly refers to the combination of renewable energy sources—such as solar, wind, hydro, and tidal energy—with storage technologies, including battery energy storage systems (BESSs), fuel cells (FCs), alongside diesel generators (DGs), gasoline power units, and biogas-based energy plants. These systems are specifically designed to minimize the reliance on DGs by prioritizing the utilization of instantly available renewable energy and stored power. Consequently, the operational lifespan of conventional generators is extended, fuel consumption is reduced, and the overall net present cost (NPC) of the system throughout its lifecycle is significantly lowered. The integration of renewable and conventional generation to address energy demands in isolated areas has been successfully applied not only in small communities but also in electric vehicles, ships, and other infrastructures equipped with advanced technologies, such as microgrids.

The dimensioning of HRES is typically categorized into two main approaches based on the variables of interest. One approach focuses on optimizing the system to minimize the NPC while maintaining a specified level of reliability. Alternatively, the system can be designed to minimize both the NPC and greenhouse gas (GHG) emissions. The former is technically referred to as mono-objective optimization, while the latter is known as multi-objective optimization. This research places particular emphasis on mono-objective techniques.

The production of energy conversion devices for renewable energy, such as photovoltaic (PV) panels and wind turbines (WTs), has grown significantly, leading to a wide variety of brands available on the market. This proliferation poses challenges for the design process from a computational perspective, as the extensive range of PV modules, WTs, and BESSs greatly increases the number of potential combinations that must be evaluated to identify the optimal solution. To manage this complexity, researchers frequently employ modern optimization approaches (MOAs).

The widespread adoption of renewable energy has spurred the development of numerous computational tools for sizing HRESs, with

* Corresponding author.
E-mail addresses: lujano.juan@unizar.es (J.M. Lujano-Rojas), rdufo@unizar.es (R. Dufo-López), jsartal@unizar.es (J.S. Artal-Sevil), egarciap@unizar.es (E. García-Paricio).

https://doi.org/10.1016/j.egyr.2025.11.047
Received 24 November 2024; Received in revised form 8 April 2025; Accepted 12 November 2025
Available online 18 November 2025

HOMER Pro® being a notable example. This software includes modules that integrate various energy sources and storage systems, such as biomass generation, hydropower, combined heat and power generation, advanced BESSs, and hydrogen storage. Additionally, it enables users to perform multi-year analyses and conduct complex studies by interfacing with computational languages like MATLAB®.

HOMER Pro® is extensively utilized in studies on renewable energy integration worldwide. Hussam et al. (2024). used HOMER Pro® to design a system in Kuwait, analyzing three configurations comprising PV panels, WTs, FCs, and a BESS. Both isolated and grid-connected operating conditions were examined, with the study concluding that integrating solar PV energy and wind generation into the grid was the most advantageous architecture. This configuration yielded a levelized cost of energy (LCOE) of $0.539/kWh and a hydrogen production cost of $6.85/kg. In isolated operating mode, a hydrogen production cost of $8/kg was observed, primarily due to the high investment costs. Additionally, a sensitivity analysis revealed a significant dependence on the cost of PV panels.

Khalid et al. (2024). designed an HRES for Pakistan utilizing PVsyst® and HOMER Pro®, incorporating a PV generator, a BESS, and a DG. The researchers validated their findings through hardware-in-the-loop testing and observed high efficiency and reliability under varying environmental conditions, including fluctuations in solar irradiance and temperature. The authors reported an estimated LCOE ranging from 0.102 $/kWh to 0.572 $/kWh, depending on the solar irradiance levels.

Using HOMER Pro®, Ozturk et al. (2024). developed an HRES consisting of PV modules, a BESS, and a DG, evaluating its performance across various regions of Türkiye with diverse load profiles. The system operates in conjunction with the main grid under a time-of-use tariff structure. During the optimization process, the researchers prioritized profit maximization as the primary objective while imposing a constraint to limit GHG emissions. To assess the robustness of the design, they performed a sensitivity analysis on inflation and discount rates, uncovering substantial variations in PV generator capacity and emphasizing the critical importance of economic stability.

Al-Odat et al. (2024). developed a grid-connected HRES using HOMER Pro® to meet the energy demands of a cement factory in Kuwait. The system incorporated PV modules and WTs for power generation. Based on their findings, the authors highlighted the economic and environmental benefits of transitioning to clean energy sources, achieving an LCOE of 0.082 $/kWh—approximately 32 % lower than that of a conventional generation system.

In addition to HOMER Pro® and PVsyst®, researchers worldwide have utilized advanced MOAs to optimize HRES designs effectively. Li et al. (2024a). proposed a methodology to improve the HRES design process by incorporating the specific layout of solar PV panels and WTs into the optimization, with system power production as the primary objective. The authors implemented the exponential slime mould algorithm, which demonstrated superior performance compared to other MOAs, such as particle swarm optimization (PSO) and the grey wolf optimizer (GWO).

Natural phenomena continually inspire scientists to develop advanced MOAs, which are subsequently employed in the design of HRESs. Over the past year, promising MOAs have been incorporated into the extensive suite of optimization techniques used for HRES sizing. Menesy et al. (2024). applied three MOAs for mono-objective optimization—artificial rabbit optimization, GWO, and the whale optimization algorithm (WOA)—to design a system in Saudi Arabia that integrated multiple PV modules, WTs, and an FC. Additionally, the researchers employed PSO as a benchmark for comparison. The results revealed that artificial rabbit optimization outperformed GWO, WOA, and PSO, achieving an LCOE of 0.4412 $/kWh, compared to 0.4438 $/kWh, 0.4443 $/kWh, and 0.44378 $/kWh for GWO, WOA, and PSO, respectively. Furthermore, the investigators conducted the optimization process 50 times to determine the optimal configuration within the search space. They then assessed the performance of each algorithm using standard deviation and other relevant metrics.

Kohole et al. (2024). applied a representative selection of MOAs to the design of HRESs. The algorithms evaluated included the imperialist competitive algorithm, vibrating particles system, big bang-big crunch algorithm, charged system search algorithm, and artificial bee colony (ABC) algorithm. The study focused on optimizing the sizing of a system comprising a PV generator, WTs, a DG, and an FC under light, medium, and heavy load scenarios. The results indicated that for the light load scenario, the vibrating particles system achieved the lowest NPC, followed by the big bang-big crunch algorithm, ABC, imperialist competitive algorithm, and charged system search. For the medium load scenario, the vibrating particles system also identified the optimal configuration, followed by ABC, big bang-big crunch algorithm, imperialist competitive algorithm, and charged system search. Similarly, in the heavy load scenario, the vibrating particles system outperformed the other algorithms, followed by the big bang-big crunch algorithm, ABC, charged system search, and imperialist competitive algorithm. Regarding the LCOE, the estimated values were $2.384/kWh, $1.753/kWh, and $1.087/kWh for the light, medium, and heavy load scenarios, respectively. It is important to highlight that the scientists repeated the optimization routine 50 times to determine the optimal HRES structure.

Ma et al. (2024). proposed a model that incorporates various scenarios of natural resource availability generated using advanced deep learning techniques, specifically the Wasserstein generative adversarial network with gradient penalty. The study focused on an HRES comprising PV modules, WTs, and a BESS optimized using the sparrow search algorithm. The effectiveness of the sparrow search algorithm was validated through a case study in China, where the integration of a BESS led to a reduction in clean energy curtailment by 3.6–14.7 % compared to the scenario without storage integration.

Mohamed et al. (2024). optimized the sizing of an HRES operating in Egypt using the walrus optimization algorithm, coati optimization algorithm, and osprey optimization algorithm, considering PV modules, WTs, and FCs. PSO and GWO were employed as benchmarks for comparison. The results showed that the walrus optimization algorithm outperformed the coati optimization algorithm, osprey optimization algorithm, GWO, and PSO in terms of LCOE, achieving values of 0.51758 $/kWh, 0.51766 $/kWh, 0.51772 $/kWh, 0.51781 $/kWh, and 0.54583 $/kWh, respectively. As part of their methodology, the authors conducted the optimization process 20 times to identify a high-quality HRES configuration.

Coban (2024) designed an HRES for installation in Türkiye using the Nelder-Mead simplex search method. The study considered PV generation, WTs, a BESS, and a DG. The researchers highlighted the critical role of the BESS in managing the variability of solar and wind resources, as well as its contribution to the economic viability of the project, achieving an LCOE of 0.63 €/kWh.

Yuan et al. (2024). developed a sizing model utilizing the firefly algorithm to optimize a system comprising PV generation, WTs, and a BESS. The modeling process accounted for BESS degradation and the uncertainties associated with renewable resources. The authors reported that the cost attributed to resource uncertainty ranged between 4.2 % and 5 % of the cost estimated using a deterministic model.

Huang et al. (2024). designed an HRES incorporating WTs and FCs. To achieve this, the authors developed the hybrid golden search algorithm and benchmarked its performance against other methods, including fuzzy logic and optimization, ABC, and the original golden search algorithm. The results indicated that the hybrid golden search algorithm outperformed the benchmark approaches. Moreover, the researchers conducted a sensitivity analysis on system reliability, revealing that a reduction in reliability from 99 % to 97 % led to an approximate 7.3 % decrease in the NPC. Specifically, the cost associated with the WTs decreased by 6 %, while the cost attributed to the FCs declined by 21 %. Additionally, the researchers performed extensive experiments, repeating the optimization routine 30 times with varying

iteration counts to identify the optimal system configuration.

Roy et al. (2024). designed an HRES for installation in India. The study considered a PV generator, WTs, a BESS, and a BG generator. The researchers examined a constrained portion of the search space, evaluating all possible combinations—1295 in total—and developed a database focused on the LCOE. Subsequently, they trained several artificial neural networks, including narrow, medium, and wide ReLU architectures, providing a contemporary perspective on HRES analysis through machine learning models.

Superchi et al. (2025). analyzed an HRES comprising WTs, PV modules, a BESS based on lithium-ion batteries, and FCs. They validated the effectiveness of their model through a comparative analysis with the actual conditions of a Greek island. Specifically, the researchers focused on the effects of degradation, developing a model that reduces computational effort by 88.5 % with a precision loss of only 0.015 %. The study highlighted the benefits of hydrogen integration as seasonal storage, enabling a 17.5 % reduction in NPC. Furthermore, they found that neglecting BESS degradation effects resulted in an estimation error of 10.2 % in the NPC. Finally, the authors integrated their model into a stochastic optimization framework based on differential evolution and conducted a comparative study with PSO, yielding favorable results.

Yahya et al. (2024). designed an HRES for operation in Libya, consisting of PV panels, WTs, a BESS, and FCs. The authors employed several MOAs, including PSO, WOA, ant colony optimization, and genetic algorithms (GAs). They observed that WOA and ant colony optimization delivered the best results, depending on specific environmental conditions. This study highlights the advantages of adopting hydrogen technology as a storage system and provides valuable insights into the implementation of MOAs for HRES sizing.

Dawsari et al. (2024). designed an HRES in Saudi Arabia, powered by PV modules, WTs, a BESS, and a DG. The researchers proposed the use of the dwarf mongoose optimization algorithm and performed a comparative analysis with the sparrow search algorithm and the WOA in terms of LCOE. The results demonstrated the effectiveness of the dwarf mongoose optimization algorithm, achieving an LCOE of 0.199 $/kWh. Furthermore, the authors repeated the optimization process 10 times, trying to identify the global optimum.

Ali and Mohammed (2024) designed an HRES for a location in South Africa, incorporating PV panels, WTs, FCs, and a BESS. The authors proposed the use of quasi-optimal control, a method that adjusts the system architecture over the project's lifetime. This approach reduces idle capacity and enhances the adaptability of the system design to evolving demand, thereby significantly improving computational efficiency.

Roshani et al. (2024) designed an off-grid residential community in the United States equipped with PV generation, WTs, and FCs. The authors proposed the use of response surface methodology as the optimization procedure and utilized TRNSYS® software for system simulations. Their results demonstrated a significant reduction in NPC and GHG emissions.

Loh and Nfah (2024) designed an HRES in Cameroon, accounting for both residential and industrial load profiles. The researchers proposed a two-step methodology for system dimensioning. In the first step, an analytical approach was utilized to estimate the sizes of the BESS, DG, and PV modules. In the second step, three MOAs—ABC, GA, and PSO—were integrated to determine the optimal system configuration. The analysis compared isolated and grid-connected configurations, with results indicating that the grid-connected configuration was more advantageous, achieving an LCOE of 0.1441 €/kWh.

Li et al. (2024b). designed a system for deployment in Antarctica, incorporating WTs, PV modules, a BESS, a DG, and a thermal load. The authors developed an optimization model that addresses the uncertainty of environmental resources and load demand using a scenario-generation method based on credibility theory. After estimating scenarios for both extreme and typical conditions, these scenarios were integrated into a fuzzy credibility-constrained stochastic-robust optimization framework to determine the optimal system configuration. The results of a case study demonstrated that their approach yields a system structure with an LCOE of 0.16 $/kWh, representing a 33 % reduction compared to results obtained using conventional stochastic techniques.

Liu et al. (2024). proposed an enhanced version of the dung beetle optimization algorithm and demonstrated its effectiveness in designing an HRES comprising PV panels, WTs, a BG, and a BESS utilizing various technologies, including lithium-ion batteries, lead-acid batteries (LABs), and nickel-iron batteries. The study concluded that the optimal system configuration includes a nickel-iron battery-based storage system and multiple PV modules, with no WTs, achieving an LCOE of 0.3607 $/kWh. Additionally, the authors conducted 10 independent optimization routines to identify the global optimum.

Wang et al. (2024). proposed the improved subtraction-average-based optimizer and applied it to the optimal design of an HRES in China, incorporating WTs, PV panels, and FCs. The enhanced features of improved subtraction-average-based optimizer enabled the system designer to achieve a configuration that was 12 % superior to that obtained with the original algorithm. To ensure the identification of the global optimum, the authors repeated the optimization process 20 independent times.

Bourek et al. (n.d.). designed an HRES using a GA for a location in Algeria, while PSO was employed for comparative purposes. The scientists considered WTs, PV panels, and FCs, obtaining a configuration with LCOE equal to 0.18 $/kWh.

Traditional MOAs, including GA, PSO, golden search algorithm, differential evolution, ant colony optimization, and ABC, continue to be widely utilized due to their proven effectiveness in addressing complex optimization problems. Furthermore, recently developed techniques such as GWO, WOA, imperialist competitive algorithm, firefly algorithm, exponential slime mould algorithm, artificial rabbit optimization, vibrating particles system, big bang-big crunch algorithm, charged system search, sparrow search algorithm, walrus optimization algorithm, coati optimization algorithm, osprey optimization algorithm, hybrid golden search algorithm, fuzzy logic and optimization, dwarf mongoose optimization algorithm, response surface methodology, dung beetle optimization, and improved subtraction-average-based optimizer have demonstrated exceptional efficacy in the design of HRESs on a global scale.

It is important to emphasize that these methods demand significant computational resources. Researchers enhance their performance by incorporating and refining search operators, thereby improving their exploration and exploitation capabilities. Nevertheless, these methods remain susceptible to stagnation around a local optimum, an issue stemming from the inherent uncertainty of the search process. In other words, MOAs are initialized randomly, which can lead to different local optima across independent runs. To address this challenge, Menesy et al. (2024), Kohole et al. (2024), Mohamed et al. (2024), Huang et al. (2024), Dawsari et al. (2024), Wang et al. (2024). executed the optimization program 50, 50, 20, 30, 10, and 20 times, respectively, to identify the lowest NPC among all local minima. However, they did not provide any information regarding the quality of the solution in terms of its optimality.

The updated literature review presented above highlights significant efforts to develop a highly efficient optimization algorithm capable of reaching the global optimum. Researchers continue to pursue such an algorithm, and these efforts are ongoing. In this paper, we proposed the orchard algorithm (OA), a recently developed optimization method, for the optimal sizing of HRESs. The effectiveness of OA is demonstrated by designing a hypothetical system for installation in Nigeria, with the results compared to those obtained using a GA. To the best of our knowledge, the performance of OA in the optimal dimensioning of autonomous HRESs has not been previously investigated. Therefore, we believe it is worthwhile to analyze the capabilities of this algorithm, given the computational complexity of HRES design, which is directly

linked to the wide variety of WTs, PV panels, and BESSs available from manufacturers worldwide.

Concerning the BESS, we consider LABs, including their aging process through the weighted *Ah* throughput model. Otherwise, we also consider the intrinsic uncertainty of the MOAs, repeating the optimization routine 100 times and estimating the probability of finding an unseen local optimum. The remainder of this paper is organized as follows: 2 describes the HRES model, 3 explains the implementation of OA, 4 demonstrates OA's capabilities with a rural electrification project, and 5 presents the main conclusions.

2. Model of the hybrid renewable energy system

The basic HRES is equipped with wind and solar PV generators, an LAB, a power converter, and a backup generator powered by conventional fuels, such as gasoline or diesel. Fig. 1 illustrates the general structure of an HRES designed for rural electrification.

The management strategy primarily aims to reduce the operational time of the backup generator, thereby extending its lifespan, lowering fuel consumption, and consequently decreasing GHG emissions. To achieve this, wind and solar PV generators are integrated, while the BESS stores surplus energy, which can be consumed later when wind and solar resources are unavailable. This concept forms the core of the load-following strategy, implemented by the energy management system.

With reference to the information presented in Fig. 1, the index $t = 1, \ldots, T$ represents the simulation time, $z = 1, \ldots, Z$ refers to the wind turbine manufacturers, $v = 1, \ldots, V$ identifies the PV panel manufacturers, $m = 1, \ldots M$ specifies the battery manufacturers, and $y = 1, \ldots, Y$ denotes the backup generator manufacturers.

According to this nomenclature, $P_{W(t,z)}$ represents the wind generation at time t for wind turbine manufacturer z, $P_{PV(t,v)}$ represents the PV generation at time t for panel manufacturer v, $P_{BT(t,m)}$ denotes the charging or discharging power at time t for battery manufacturer m, $P_{G(t,y)}$ refers to the power of the backup unit at time t for generator manufacturer y, and $P_{L(t)}$ represents the load demand at time t.

2.1. Wind generation

Typically, wind turbine manufacturers provide information on the energy conversion process through a power curve, which relates wind speed to power output. The power curve can be read continuously using a linear interpolation routine, a feature commonly available in many computational languages. The power production of a single turbine at time t for manufacturer z is represented by the variable $p_{w(t,z)}$, while the total power output of the generator (denoted as $P_{W(t,z)}$ in Fig. 1) is obtained by connecting multiple turbines in parallel.

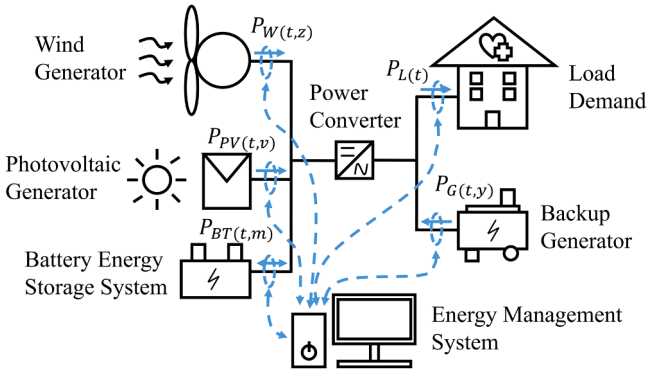

Fig. 1. Structure of a typical hybrid renewable energy system.

2.2. Solar photovoltaic generator

PV panel manufacturers provide users with datasheets containing essential parameters to estimate power production. Eqs. (1) and (2) offer a reasonable approximation of the power generation for a single panel ($p_{pv(t,v)}$) (Lambert et al., 2006):

$$T_{C(t)} = T_{A(t)} + \left(\frac{NOCT_{(v)} - 20 \quad ^\circ C}{800\text{W/m}^2}\right) G_{(t)}, \tag{1}$$

$$p_{pv(t,v)} = P_{STC(v)} \left\{ \frac{G_{(t)}}{1000\text{W/m}^2} \left[1 + \alpha_{PV(v)} (T_{C(t)} - 25 \quad ^\circ C)\right] \right\}, \tag{2}$$

where $NOCT_{(v)}$ represents the nominal operating cell temperature for manufacturer v, $\alpha_{PV(v)}$ is the temperature coefficient of power for manufacturer v, and $P_{STC(v)}$ is the power output under standard test conditions for manufacturer v. These parameters are typically provided by the manufacturers; however, variables related to environmental conditions, such as ambient temperature $T_{A(t)}$ and solar irradiance $G_{(t)}$, must be estimated for the location of interest. Using the ambient temperature, the PV cell temperature $T_{C(t)}$ can be estimated using Eq. (1). Once the power output of a single PV $p_{pv(t,v)}$ has been estimated, the total power generation $P_{PV(t,v)}$ can be calculated by scaling the results based on the number of strings connected in parallel.

2.3. Battery energy storage system

A key element of the HRES is the BESS, as it provides a certain degree of dispatchability to wind and solar PV generation. In rural electrification projects, the storage device is usually based on lead-acid technology. For this reason, we place special emphasis on this technology. Accordingly, we implement the weighted *Ah* throughput model, which is briefly described in the following sub-sections.

2.3.1. General-purpose model of typical lead-acid battery cell

The voltage estimation of an LAB cell is often calculated using Shepherd's equation, which accounts for the effects of charging or discharging current and the state of charge (SOC). Eqs. (3) and (4) (Schiffer et al., 2007; Andersson, 2006; Bindner et al., 2005) present the voltage for charging and discharging, respectively.

$$U_{(t,m)} = U_{0(m)} - g_{(m)} DOD_{(t,m)} + R^c_{(t,m)} \left(\frac{I_{(t,m)}}{C_{10(m)}}\right) + R^c_{(t,m)} M_{c(m)} \left(\frac{I_{(t,m)}}{C_{10(m)}}\right) \left(\frac{SOC_{(t,m)}}{C_{c(m)} - SOC_{(t,m)}}\right) \forall I_{(t,m)} > 0, \tag{3}$$

$$U_{(t,m)} = U_{0(m)} - g_{(m)} DOD_{(t,m)} + R^d_{(t,m)} \left(\frac{I_{(t,m)}}{C_{10(m)}}\right) + R^d_{(t,m)} M_{d(m)} \left(\frac{I_{(t,m)}}{C_{10(m)}}\right) \left(\frac{DOD_{(t,m)}}{C^d_{(t,m)} - DOD_{(t,m)}}\right) \forall I_{(t,m)} \leq 0. \tag{4}$$

where $U_{(t,m)}$ and $I_{(t,m)}$ represent the cell voltage and current at time t for manufacturer m, respectively. During charging, the condition $I_{(t,m)} > 0$ is satisfied, while discharging occurs when $I_{(t,m)} \leq 0$. $SOC_{(t,m)}$ and $DOD_{(t,m)}$ denote SOC and depth of discharge at time t for manufacturer m, respectively. $C_{10(m)}$ is the 10-hour discharge capacity for manufacturer m, $U_{0(m)}$ is the open-circuit voltage for manufacturer m, and $g_{(m)}$ represents the variation of the open-circuit voltage with depth of discharge. $C_{c(m)}$ and $C^d_{(t,m)}$ are the normalized capacities during charging and discharging, respectively, for manufacturer m. $M_{c(m)}$ and $M_{d(m)}$ are the charge transfer resistances during charging and discharging, respectively, for manufacturer m, while $R^c_{(t,m)}$ and $R^d_{(t,m)}$ represent the resistances during charging and discharging, respectively, for manufacturer m.

Regarding SOC at a specific time and for a particular manufacturer

($SOC_{(t,m)}$), it is calculated according to Eq. (5) (Schiffer et al., 2007; Andersson, 2006; Bindner et al., 2005):

$$SOC_{(t,m)} = SOC_{(t-\Delta t,m)} + \int_{t-\Delta t}^{t} \left\{ \frac{I_{(\tau,m)} - I^{G}_{(\tau,m)}}{C_{10(m)}} \right\} d\tau, \tag{5}$$

where Δt is the simulation time step, assumed to be 1 h, and $I^{G}_{(t,m)}$ is the gassing current at time t for manufacturer m, estimated using Eq. (6) (Schiffer et al., 2007; Andersson, 2006; Bindner et al., 2005):

$$I^{G}_{(t,m)} = \left(\frac{C_{10(m)}}{100}\right)\left(I^{G}_{0(t,m)}\right)\exp\left(C_{U(m)}\left[U_{(t,m)} - U^{G}_{0(m)}\right] + C_{T(m)}\left[T_{A(t)} - T^{G}_{0(m)}\right]\right) \forall I_{(t,m)} > 0. \tag{6}$$

where, for manufacturer m, $C_{U(m)}$ and $C_{T(m)}$ are the voltage and temperature coefficients of gassing, respectively, while $U^{G}_{0(m)}$ and $T^{G}_{0(m)}$ are the reference voltage and temperature for the gassing process.

2.3.2. Modelling of the positive grid corrosion process

The corrosion process can be described using Shepherd's equation, with the parameters appropriately set to calculate the corrosion voltage during charging and discharging, as shown in Eqs. (7) and (8) (Schiffer et al., 2007; Andersson, 2006; Bindner et al., 2005):

$$U^{c}_{(t,m)} = U^{c}_{0(m)} - \left(\frac{10}{13}\right) g_{(m)} DOD_{(t,m)} + R^{c}_{(t,m)}\left(\frac{I_{(t,m)}}{2C_{10(m)}}\right) + R^{c}_{(t,m)} M_{c(m)} \left(\frac{I_{(t,m)}}{2C_{10(m)}}\right)\left(\frac{SOC_{(t,m)}}{C_{c(m)} - SOC_{(t,m)}}\right) \forall I_{(t,m)} > 0, \tag{7}$$

$$U^{c}_{(t,m)} = U^{c}_{0(m)} - \left(\frac{10}{13}\right) g_{(m)} DOD_{(t,m)} + R^{d}_{(t,m)}\left(\frac{I_{(t,m)}}{2C_{10(m)}}\right) + R^{d}_{(t,m)} M_{d(m)} \left(\frac{I_{(t,m)}}{2C_{10(m)}}\right)\left(\frac{DOD_{(t,m)}}{C^{d}_{(t,m)} - DOD_{(t,m)}}\right) \forall I_{(t,m)} \leq 0, \tag{8}$$

where $U^{c}_{(t,m)}$ is the corrosion voltage, and $U^{c}_{0(m)}$ is the corrosion voltage when the cell is fully charged, both for manufacturer m at time t. The behavior of the corrosion layer can be estimated using Eqs. (9)-(12) (Schiffer et al., 2007; Andersson, 2006; Bindner et al., 2005):

$$\Delta\omega_{(t,m)} = \begin{cases} k_{sp}\left(b^{0.6}\right) | b = \left[\Delta\omega_{(t-\Delta t,m)} / \left(k_{sp}\right)\right]^{\frac{1}{0.6}} + \Delta t; U^{c}_{(t,m)} < 1.74 \\ \Delta\omega_{(t-\Delta t,m)} + \left(k_{sp}\right)\Delta t; U^{c}_{(t,m)} \geq 1.74 \end{cases}, \tag{9}$$

$$\Delta R_{(t,m)} = \Delta R_{\max}\left(\frac{\Delta\omega_{(t,m)}}{\Delta\omega_{\max(m)}}\right), \tag{10}$$

$$\Delta C^{c}_{(t,m)} = \Delta C^{c}_{\max}\left(\frac{\Delta\omega_{(t,m)}}{\Delta\omega_{\max(m)}}\right), \tag{11}$$

$$\Delta\omega_{\max(m)} = 365 \times 24 \times \left(FL_{(m)}\right)\left(k^{sp}_{\max(m)}\right), \tag{12}$$

where $\Delta\omega_{(t,m)}$ and $\Delta\omega_{\max(m)}$ are the corrosion layer thickness and its maximum value, k_{sp} and $k^{sp}_{\max(m)}$ are the speed coefficients of the corrosion process at float voltage and their maximum values, $\Delta R_{(t,m)}$ and $\Delta R_{\max}$ are the increments in internal resistance due to corrosion and their maximum values, $\Delta C^{c}_{(t,m)}$ and $\Delta C^{c}_{\max}$ represent capacity loss and its maximum value, and $FL_{(m)}$ is the battery float life for manufacturer m.

2.3.3. Modelling of the active mass degradation phenomenon

Active mass degradation is estimated using a set of factors related to SOC, the operating time at a low SOC, the discharging current, and incomplete or insufficient charging cycles. These factors are defined in Eqs. (13)-(16) and are complemented by the information in Fig. 2. Upon examining Fig. 2, we observe the partial and full charging operations, defined by the limit SOC value $SOC^{\max}_{\lim}$, assumed to be 0.9.

For a battery from manufacturer m, the operating time at a low SOC is measured by the quantity $\min\{SOC_{(\tau,m)} | \tau \in [t_Y, t]\}$ and the time interval $t - t_Y$. These definitions and operating conditions are incorporated into the SOC factor $f^{soc}_{(t,m)}$, as presented in Eqs. (13) and (14) (Schiffer et al., 2007; Andersson, 2006; Bindner et al., 2005):

$$f^{soc}_{(t,m)} = 1 + \left[c^{soc}_{0(m)} + c^{soc}_{\min(m)}\left(1 - \min\{SOC_{(\tau,m)} | \tau \in [t_Y, t]\}\right) f^{I}_{(t,m)} \Delta t^{soc}_{(t)}\right], \tag{13}$$

$$\Delta t^{soc}_{(t)} = t - t_Y, \tag{14}$$

where, for manufacturer m, $c^{soc}_{0(m)}$ and $c^{soc}_{\min\,(m)}$ are the slope and minimum SOC value, $\Delta t^{soc}_{(t)}$ is the time since the last complete charge, and $f^{I}_{(t,m)}$, the current factor introduced to quantify the effects of the discharging current, is estimated through Eq. (15) (Schiffer et al., 2007; Andersson, 2006; Bindner et al., 2005):

$$f^{I}_{(t,m)} = \left(\sqrt{\frac{I_{r(m)}}{I^{1th}_{(t,m)}}}\right)\left(\sqrt[3]{\exp\left(\frac{q_{(t,m)}}{3.6}\right)}\right), \tag{15}$$

where $I_{r(m)}$, for manufacturer m, is the reference current value, $I^{1th}_{(t,m)}$ is the charging current measured when partial cycling begins, and $q_{(t,m)}$ is the number of incomplete charging cycles, computed by considering the weighting $\Delta q_{(t,m)}$ from Eq. (16) (Schiffer et al., 2007; Andersson, 2006; Bindner et al., 2005):

$$\Delta q_{(t,m)} = \frac{0.0025 - \left(0.95 - \max\{SOC_{(\tau,m)} | \tau \in [t_X, t_Y]\}\right)^2}{0.0025}. \tag{16}$$

The stratification factor ($f^{ST}_{(t,m)}$) incorporates the impact of gassing and diffusion phenomena, as simulated by Eqs. (17)-(21) for manufacturer m. According to Eq. (17), the difference between the increase in acid stratification ($\Delta f^{+}_{(\tau,m)}$) associated with partial charging and the decrease in acid stratification ($\Delta f^{-}_{(\tau,m)}$) due to the gassing process is crucial for accurately evaluating battery lifetime (Schiffer et al., 2007; Andersson, 2006; Bindner et al., 2005).

$$f^{ST}_{(t,m)} = f^{ST}_{(t-\Delta t,m)} + \int_{t-\Delta t}^{t} \left(\Delta f^{+}_{(\tau,m)} - \Delta f^{-}_{(\tau,m)}\right) d\tau, \tag{17}$$

$$\Delta f^{+}_{(t,m)} = C_{P(m)}\left(1 - \min\{SOC_{(\tau,m)} | \tau \in [t_Y, t]\}\right)\exp\left(-3 f^{ST}_{(t,m)}\right)\left(\frac{\left|I^{d}_{(t,m)}\right|}{I_{r(m)}}\right), \tag{18}$$

$$\Delta f^{-}_{G(t,m)} = C_{M(m)}\sqrt{\frac{100}{C_{10(m)}}}\left(\frac{I^{G}_{0(t,m)}}{I^{G}_{0(m)}}\right)\exp\left(C_{U(m)}\left[U_{(t,m)} - U_{r(m)}\right] + C_{T(m)}\left[T_{A(t)} - T^{G}_{0(m)}\right]\right), \tag{19}$$

$$\Delta f^{-}_{D(t,m)} = \frac{8 D_{Z(m)}}{\left(Z_{D(m)}\right)^2} f^{ST}_{(t-\Delta t,m)} 2^{(T_{A(t)} - 293.15)/10}, \tag{20}$$

$$\Delta f^{-}_{(t,m)} = \Delta f^{-}_{D(t,m)} + \Delta f^{-}_{G(t,m)}. \tag{21}$$

Regarding the variables in Eqs. (17)-(21) for manufacturer m, $I^{d}_{(t,m)}$ is the discharging current, $C_{P(m)}$ and $C_{M(m)}$ are parameters related to the increase and decrease of acid stratification, respectively, $U_{r(m)}$ is the reference voltage for the acid stratification process, $D_{Z(m)}$ is a parameter of the diffusion process, and $Z_{D(m)}$ represents the typical cell height. $\Delta f^{-}_{G(t,m)}$ and $\Delta f^{-}_{D(t,m)}$ correspond to the reduction of acid stratification due to gassing and diffusion, respectively. The net effect on acid stratification is captured in the acid stratification factor ($f^{A}_{(t,m)}$), as described in Eq. (22) (Schiffer et al., 2007; Andersson, 2006; Bindner et al., 2005).

$$f^{A}_{(t,m)} = 1 + f^{ST}_{(t,m)} \sqrt{\frac{I_{r(m)}}{I^{1th}_{(t,m)}}}. \tag{22}$$

Subsequently, the SOC and acid stratification factors ($f^{soc}_{(t,m)}$ and $f^{A}_{(t,m)}$ for manufacturer m) are used to calculate the weighted Ah ($Z^{w}_{(t,m)}$), as shown in Eq. (23) (Schiffer et al., 2007; Andersson, 2006; Bindner et al., 2005).

$$Z^{w}_{(t,m)} = \frac{1}{C_{10(m)}} \int_0^t \left| I^{d}_{(t,m)} \right| f^{soc}_{(t,m)} f^{A}_{(t,m)} dt. \tag{23}$$

Subsequently, the weighted Ah ($Z^{w}_{(t,m)}$ for manufacturer m) is used to calculate the capacity loss due to degradation ($\Delta C^{d}_{(t,m)}$), as indicated in Eq. (24) (Schiffer et al., 2007; Andersson, 2006; Bindner et al., 2005).

$$\Delta C^{d}_{(t,m)} = \Delta C^{d}_{\max(m)} \exp\left(-C_{Z(m)} \left\{ 1 - \frac{Z^{w}_{(t,m)}}{1.6[Z_{I(m)}]} \right\} \right), \tag{24}$$

where, for manufacturer m, $\Delta C^{d}_{(t,m)}$ and $\Delta C^{d}_{\max(m)}$ represent the capacity loss due to degradation and its maximum value, $C_{Z(m)}$ is a degradation-related coefficient, and $Z_{I(m)}$ is the number of standard operating cycles.

Using the results from the computational model described above, we calculate the updated values for manufacturer m, including the charging and discharging resistances ($R^{c}_{(t,m)}$ and $R^{d}_{(t,m)}$), the gassing current ($I^{G}_{0(t,m)}$), and the battery capacity ($C^{d}_{(t,m)}$), as shown in Eqs. (25)-(28) (Schiffer et al., 2007; Andersson, 2006; Bindner et al., 2005).

$$R^{c}_{(t,m)} = R^{c}_{(0,m)} + \Delta R_{(t,m)} \tag{25}$$

$$R^{d}_{(t,m)} = R^{d}_{(0,m)} + \Delta R_{(t,m)} \tag{26}$$

$$I^{G}_{0(t,m)} = I^{G}_{0(m)} + \Delta I^{G}_{0(m)} \left(\frac{\Delta R_{(t,m)}}{\Delta R_{\max(m)}} \right) \tag{27}$$

$$C^{d}_{(t,m)} = C^{d}_{(0,m)} - \Delta C^{c}_{(t,m)} - \Delta C^{d}_{(t,m)} \tag{28}$$

Fig. 3 provides a brief summary of the general procedure for estimating battery lifetime for manufacturer m, as previously described in Eqs. (3)-(28).

2.4. Power converter

The power converter is responsible for converting direct current signals into alternating current signals, and vice versa. We represent this device in terms of its efficiency ($\eta_{conv(t)}$) at each time t, as shown in Eq. (29) (Rampinelli et al., 2014).

$$\eta_{conv(t)} = \frac{P_{conv(t)}}{\xi_{conv} \times P^{\max}_{conv} + \lambda_{conv} \times P_{conv(t)}}, \tag{29}$$

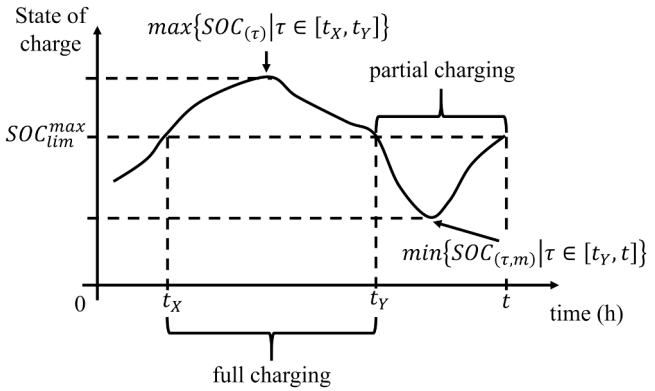

Fig. 2. Illustration of the partial and full charging conditions.

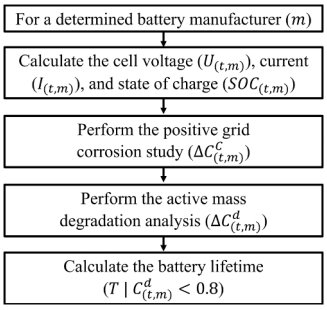

Fig. 3. Weighted Ah throughput model implementation.

where ξ_{conv} and λ_{conv} are model coefficients, $P^{\max}_{conv}$ is the maximum power of the converter, and $P_{conv(t)}$ is the power converted at time t. It is important to note that Eq. (29) simplifies a more complex expression. Further details can be found in (Rampinelli et al., 2014).

2.5. Backup generator

The key variable of interest regarding the operation of the backup generator is its fuel consumption, which is typically estimated using Eq. (30).

$$F_{g(t,y)} = \gamma_{g(y)} \times P^{\max}_{g(y)} + \chi_{g(y)} \times P_{g(t,y)}, \tag{30}$$

where $F_{g(t,y)}$ represents the fuel consumption at time t for manufacturer y, $\chi_{g(y)}$ and $\gamma_{g(y)}$ are model coefficients, and $P_{g(t,y)}$ and $P^{\max}_{g(y)}$ are the power generation at time t and its maximum value for manufacturer y, respectively.

3. Orchard algorithm for hybrid renewable energy system design

This paper addresses the challenge of determining an optimal combination of wind and solar PV generators, LABs, power converters, and backup generators that minimizes the NPC while ensuring a specified level of reliability. The subsequent sub-sections provide a detailed description of the problem being analyzed (Sub-3.1) and the solution methodology implemented using OA (Sub-3.2).

3.1. Defining the optimization problem

Solving the HRES design problem involves minimizing the NPC, a measure that encompasses the entire lifespan of the system. The NPC accounts for the capital and replacement costs of each system component, along with their operational and maintenance expenses. The LAB is one of the most costly elements due to its sensitivity to environmental conditions, which significantly affect its lifespan. Similarly, the backup generator is influenced by the need to operate to meet the net power demand. This demonstrates how resource variability impacts the estimation of the NPC. The vector $\boldsymbol{x}$ represents the configuration of a specific HRES system. Specifically, it encodes the combination of wind turbines, solar PV panels, LABs, and a backup generator using integer coding. This formulation constitutes a combinatorial problem, which can be expressed through Eq. (31)-(41). Eq. (31) encapsulates our objective of identifying the vector $\boldsymbol{x}$ that minimizes the NPC.

$$\min\{NPC_{(\boldsymbol{x})}\}, \tag{31}$$

The minimization process is subject to the constraints outlined in Eq. (32)-(41). The constraint in Eq. (32) is imposed to ensure a specific reliability level, represented by the energy index of unreliability (EIU) associated with the configuration given by the vector $\boldsymbol{x}$ ($EIU_{(\boldsymbol{x})}$) and the target value (EIU_{trg}). The EIU is a normalized measure of the energy not

supplied.

$$EIU_{(\boldsymbol{x})} \leq EIU_{trg}, \tag{32}$$

The constraints of Eqs. (33)-(35) are exclusively related to the LAB operation.

$$SOC_{\min(m)} \leq SOC_{(t,m)} \leq 1, \tag{33}$$

$$I_{bt(m)}^{\min} \leq I_{(t,m)} \leq I_{bt(m)}^{\max}, \tag{34}$$

$$U_{bt(m)}^{\min} \leq U_{(t,m)} \leq U_{bt(m)}^{\max}, \tag{35}$$

where $SOC_{\min\,(m)}$ represents the minimum SOC for manufacturer m, $I_{bt(m)}^{\min}$ and $I_{bt(m)}^{\max}$ denote the minimum and maximum battery current for manufacturer m, and $U_{bt(m)}^{\min}$ and $U_{bt(m)}^{\max}$ represent the minimum and maximum voltage for manufacturer m.

Eqs. (36) and (37) are introduced to ensure the safe operation of the power converter and the backup generator, respectively.

$$0 \leq P_{conv(t)} \leq P_{conv}^{\max}. \tag{36}$$

$$P_{g(y)}^{\min} \leq P_{g(t,y)} \leq P_{g(y)}^{\max}. \tag{37}$$

Eqs. (38) and (39) represent the system's power balance. Eq. (38) is expressed in terms of a single wind turbine ($p_{w(t,z)}$), PV panel ($p_{pv(t,v)}$), and battery cell ($p_{bt(t,m)}$), where j is the number of wind turbines in the farm, d is the number of strings in the PV array, and o is the number of batteries connected in parallel. $ENS_{(t)}$ and $ES_{(t)}$ represent the energy not supplied and energy surplus at time t, respectively. Similarly, Eq. (39) is formulated in terms of the wind and solar PV power variables ($P_{W(t,z)}$ and $P_{PV(t,v)}$) and the battery bank power ($P_{BT(t,m)}$), as illustrated in Fig. 1.

$$j \times p_{w(t,z)} + d \times p_{pv(t,v)} \pm o \times p_{bt(t,m)} + ENS_{(t)} - \left(P_{L(t)} + ES_{(t)}\right) = P_{g(t,y)}, \tag{38}$$

$$P_{W(t,z)} + P_{PV(t,v)} \pm P_{BT(t,m)} + ENS_{(t)} - \left(P_{L(t)} + ES_{(t)}\right) = P_{g(t,y)}, \tag{39}$$

Eqs. (40) and (41) complement the power balance expression.

$$0 \leq ENS_{(t)} \leq \infty, \tag{40}$$

$$0 \leq ES_{(t)} \leq \infty. \tag{41}$$

3.2. Orchard algorithm working principle

Eq. (42) defines the structure of a single optimization agent ($\boldsymbol{x}_{(i)}$), which is embedded within the general population ($\boldsymbol{X}$) as described by Eq. (43). Table 1 outlines how the information is organized within a single optimization agent, including the minimum ($\boldsymbol{x_{min}}$) and maximum ($\boldsymbol{x_{max}}$) values for each vector element, along with their respective physical meanings.

$$\boldsymbol{x}_{(i)} = [\,v \quad d \quad z \quad j \quad m \quad o \quad y\,] \tag{42}$$

$$\boldsymbol{X} = \begin{bmatrix} \vdots \\ \boldsymbol{x}_{(i)} \\ \vdots \end{bmatrix} \tag{43}$$

Table 1
Description of an OA agent.

Element of agent $\boldsymbol{x}_{(i)}$	$\boldsymbol{x_{min}}$	$\boldsymbol{x_{max}}$	Description
v	2	$V+1$	Index for solar panel manufacturers
d	2	$D+1$	Number of panels in parallel
z	2	$Z+1$	Index for wind turbine manufacturers
j	2	$J+1$	Number of wind turbines
m	2	$M+1$	Index for battery manufacturers
o	2	$O+1$	Number of batteries in parallel
y	2	$Y+1$	Index for generator manufacturers

It is important to note that uppercase values refer to the total number of manufacturers considered for each system device. The elements v, d, z, j, m, o, and y are integer values as previously described, while V, D, Z, J, M, O, and Y represent the maximum number of manufacturers of PV panels, the maximum number of PV strings, the maximum number of wind turbine manufacturers and their maximum quantity, the maximum number of LAB manufacturers, the maximum number of batteries in parallel, and the maximum number of backup generator manufacturers, respectively. Assigning a value of one as the minimum allowable value ($\boldsymbol{x_{min}}$) corresponds to the option of excluding the respective device from the HRES configuration. The implementation of the OA algorithm for HRES design is detailed in the following sub-sections.

3.2.1. Creation of an orchard

First, it is necessary to specify the number of optimization agents (I), the maximum number of iterations (K), the weighting parameters α and β, the wind speed and solar irradiance time series, the load demand time series, the target EIU, the rating voltage, the acquisition costs of each system component, the fuel price, and economic parameters such as interest and inflation rates. This information enables us to, on one hand, search for a high-quality solution using OA, and on the other, calculate the NPC for a specific combination of system devices. Additionally, we must create the matrix $\boldsymbol{f}$ to store the objective function value (NPC) of each agent at each iteration ($k = 1, \ldots, K$). Consequently, $\boldsymbol{f}$ will have I rows and K columns.

Before applying the OA, it is necessary to initialize it by generating a population using an integer random number generator, in combination with the information provided in Table 1, particularly the values for $\boldsymbol{x_{min}}$ and $\boldsymbol{x_{max}}$. This process yields an initial population, $\boldsymbol{X}$. Once this is established, the remaining procedures can be carried out.

3.2.2. Growth of the seedlings

This procedure is essentially a local search around the actual optimization agents. The growth of the seedlings is implemented by following the steps described as follows (Kaveh et al., 2023):

Step 1 Evaluate the population ($\boldsymbol{X}$) to determine the NPC ($NPC_{(\boldsymbol{x})}$) for each agent $\boldsymbol{x}_{(i)}$ $\forall i = 1, \ldots, I$, and identify the agent with the best performance, $\boldsymbol{x_{bst}}$. Then, proceed to Step 2.

Step 2 For each agent, $i = 1, \ldots, I$, in $\boldsymbol{X}$, randomly select three dimensions from the seven available (as shown in Table 1) and modify them by assigning a random value between the corresponding elements of $\boldsymbol{x_{min}}$ and $\boldsymbol{x_{max}}$. Then, proceed to Step 3.

Step 3 Evaluate the population $\boldsymbol{X}$ obtained in Step 2 and calculate the NPC ($NPC_{(\boldsymbol{x})}$) for each agent $\boldsymbol{x}_{(i)}$ $\forall i = 1, \ldots, I$. Then, proceed to Step 4.

Step 4 Compare the NPC values of the agents from the population in Step 1 with those from Step 3, and select the best ones. For each agent ($i = 1, \ldots, I$), compare the NPC obtained in Step 1 with that calculated in Step 3, one at a time, and retain the lower value. This process results in a new population ($\boldsymbol{X}$).

3.2.3. Screening of the seedlings

This procedure allows us to identify the promising agents. It is implemented by following these steps (Kaveh et al., 2023):

Step 1 Evaluate the population ($\boldsymbol{X}$) to determine the NPC ($NPC_{(\boldsymbol{x})}$) for each agent $\boldsymbol{x}_{(i)}$ $\forall i = 1, \ldots, I$. Then, proceed to Step 2.

Step 2 Sort the agents in ascending order based on the objective function values (NPC) obtained in Step 1. Next, assign the normalized values ($\boldsymbol{NPC}_{(i)}^{\boldsymbol{norm}}$) from Eq. (44) to each agent. Then, proceed to Step 3.

$$\boldsymbol{NPC}_{(i)}^{\boldsymbol{norm}} = \frac{I+1-i}{\sum_{\gamma=1}^{I}[I+1-\gamma]} \quad \forall \quad i = 1, \ldots, I \tag{44}$$

Step 3 Calculate the growth rate for each agent ($\boldsymbol{g}_{(i)}$) in accordance with Eq. (45). Then, proceed to Step 4.

$$\boldsymbol{g}_{(i)} = 0.6\left[\boldsymbol{f}_{(i,k)} - \boldsymbol{f}_{(i,k-1)}\right] + 0.3\left[\boldsymbol{f}_{(i,k-1)} - \boldsymbol{f}_{(i,k-2)}\right] + 0.1\left[\boldsymbol{f}_{(i,k-2)} - \boldsymbol{f}_{(i,k-3)}\right] \quad \forall \; i = 1,\ldots,I \tag{45}$$

Step 4 Sort the agents in ascending order based on the growth rate values obtained in Step 3. Then, assign the normalized values ($\boldsymbol{g}_{(i)}^{\boldsymbol{norm}}$) from Eq. (46) to each agent. Proceed to Step 5.

$$\boldsymbol{g}_{(i)}^{\boldsymbol{norm}} = \frac{I+1-i}{\sum_{\gamma=1}^{I}[I+1-\gamma]} \quad \forall \quad i = 1,\ldots,I \tag{46}$$

Step 5 Calculate the optimality index ($\lambda_{(i)}$) using the results obtained in Steps 2 and 4. Then, proceed to Step 6.

$$\lambda_{(i)} = \alpha \times \boldsymbol{NPC}_{(i)}^{\boldsymbol{norm}} + \beta \times \boldsymbol{g}_{(i)}^{\boldsymbol{norm}} \quad \forall \quad i = 1,\ldots,I \tag{47}$$

Step 6 Divide the population ($\boldsymbol{X}$) into three classes: strong ($\boldsymbol{x}_{\boldsymbol{str}}$), transition ($\boldsymbol{x}_{\boldsymbol{trn}}$), and weak ($\boldsymbol{x}_{\boldsymbol{wek}}$). These classes are determined based on the optimality index calculated in Step 5, with the strong class having the highest optimality index.

3.2.4. Grafting

This procedure focuses particularly on agents with potential for improvement, specifically those in the transition class. The grafting process is applied by following these steps (Kaveh et al., 2023):

Step 1 Calculate the number of rows (Δ) for the transition portion of the general population ($\boldsymbol{x}_{\boldsymbol{trn}}$). This can be done by computing $\lfloor 2I/3 \rfloor - \lfloor I/3 \rfloor$ or by using the relevant computational function available in many programming languages. Then, proceed to Step 2.

Step 2 Combine each agent from the transition class ($\boldsymbol{x}_{\boldsymbol{trn}}$) with one randomly selected from the strong class ($\boldsymbol{x}_{\boldsymbol{str}}$). For each agent ($\delta = 1, \ldots, \Delta$) in the transition class, generate an integer random number (σ) between 1 and the number of rows in the strong class ($\lfloor I/3 \rfloor$). Then, concatenate the portion of the agent σ $\boldsymbol{x}_{\boldsymbol{str}}(\sigma, 1 : \lfloor 7/3 \rfloor)$ with the portion $\boldsymbol{x}_{\boldsymbol{trn}}(\delta, \lfloor 7/3 \rfloor + 1 : 7)$ of agent δ.

3.2.5. Replacement and elitism

This process replaces the low-performance agents with new ones randomly selected, considering the limits presented in Table 1. It is implemented through the following steps (Kaveh et al., 2023):

Step 1 Replace the weak portion of the general population ($\boldsymbol{x}_{\boldsymbol{wek}}$) with randomly generated agents, adhering to the limits provided in Table 1 ($\boldsymbol{x}_{\boldsymbol{min}}$ and $\boldsymbol{x}_{\boldsymbol{max}}$). Then, proceed to Step 2.

Step 2 Concatenate the updated versions of the strong ($\boldsymbol{x}_{\boldsymbol{str}}$), transition ($\boldsymbol{x}_{\boldsymbol{trn}}$), and weak ($\boldsymbol{x}_{\boldsymbol{wek}}$) classes to form a new population ($\boldsymbol{X}$). Then, proceed to Step 3.

Step 3 Replace the last agent with the best-performing one (x_{bst}).

The procedures described above are applied in a specific sequence. Let $k = 1, \ldots, K$ represent each iteration. While $k \leq 4$, only the growth of the seedlings process is considered (Sub-3.2.2). Once $k > 4$, the processes of seedling growth, seedling screening (Sub-3.2.3), grafting (Sub-3.2.4), and replacement and elitism (Sub-3.2.5) are applied sequentially (Kaveh et al., 2023).

Using GA as a reference MOA, it is evident that OA—through orchard creation, seedling growth, seedling screening, grafting, replacement, and elitism—explores and exploits the search space in a more exhaustive manner than GA, which relies solely on selection, crossover, and mutation operators. However, GA incurs significantly lower computational overhead, resulting in faster execution. On one hand, OA can identify more promising solutions by allocating greater computational resources. On the other hand, GA's inherently simpler search space analysis limits the discovery of elite solutions, but offers the advantage of reduced computational cost.

4. Case study

The optimization technique proposed in this paper for the optimal sizing of an HRES is demonstrated through a hypothetical rural electrification project in Maiduguri, Nigeria (latitude 11.8712°, longitude 13.1649°). In Nigeria, over 40 % of the population lacks access to electricity. As a result, the use of kerosene and firewood for lighting and cooking remains widespread. Generally, there is a willingness among the population to transition to electricity generated from clean energy sources; however, the cost associated with this transition is prohibitive for the majority of Nigerians living in rural areas. Therefore, Nigeria presents a suitable context for testing and analyzing an optimization model intended for application in rural electrification initiatives in developing countries (Nduka, 2021). The necessary details are provided in the subsequent sub-sections.

4.1. Case study description and assumptions

The load demand profile used in this study was a typical one, as recommended in reference (Prinsloo and Dobson, 2016), with a peak value of 2.3 kW. Additionally, the voltage was set to 24 V. Data on natural resources, including wind speed, solar irradiance ($G_{(t)}$ $\forall t = 1,\ldots, T$), and ambient temperature ($T_{A(t)}$ $\forall t = 1,\ldots,T$), were obtained from the Renewables.ninja website (Renewables.ninja, 2024; Pfenninger and Staffell, 2016; Staffell and Pfenninger, 2016). The computational implementation of the simulation and optimization routines was conducted in MATLAB® on a personal computer equipped with an Intel Core® i7 CPU, 16 GB RAM, and a 64-bit operating system.

Regarding the system configuration, 25 manufacturers of solar PV panels ($V = 25$), wind turbines ($Z = 25$), LABs ($M = 25$), and backup generators ($Y = 25$) were considered. The maximum number of PV strings ($D = 15$), wind turbines ($Z = 15$), and LABs in parallel ($O = 15$) was set to 15.

The rated capacity of the solar PV panels ($P_{STC(v)}$ $\forall v = 1,\ldots,V = 25$) ranges from 50 W to 600 W, with acquisition and replacement costs between €68.97 and €133.20, respectively, while operating costs were considered negligible. The nominal operating cell temperature for all manufacturers ($NOCT_{(v)}$ $\forall v = 1, \ldots, V = 25$) was estimated to be approximately 44.61 °C, and the temperature coefficient of power ($\alpha_{PV(v)}$ $\forall v = 1,\ldots,V = 25$) was assumed to be around −0.3 %/°C.

For wind generation, the rated capacity was assumed to range from 400 W to 7000 W, with acquisition and replacement costs between €5002.021 and €11,752.67, respectively. Operating costs, on the other hand, were assumed to be 2 % of the acquisition costs annually.

LABs considered had capacities ranging from 10 Ah to 3000 Ah ($C_{10(m)}$ $\forall m = 1, \ldots, M = 25$), with acquisition and replacement costs between €93.06 and €470.398. On average, the number of cycles was 1317.076, and the float lifetime was approximately 11.192 years. The minimum SOC was set at 30 %, and the operating cost was considered negligible.

For the backup generator, nominal capacities ($P_{g(y)}^{\max}$ $\forall y = 1,\ldots,Y = 25$) ranging from 3000 W to 7000 W, powered by gasoline, were considered, with a minimum load assumption of 50 % ($P_{g(y)}^{\min} = 0.5 \times P_{g(y)}^{\max}$ $\forall y = 1, \ldots, Y = 25$). Acquisition and replacement costs were assumed to be between €6356.732 and €14,930.732. The lifetime and operating cost were estimated at 750 h and €0.25 per hour, respectively. The parameters for gasoline consumption ($\gamma_{g(y)}$ and $\chi_{g(y)}$ $\forall y = 1,\ldots,Y = 25$) were derived from manufacturers' data. Key variables for the NPC calculation are presented in Table 2.

4.2. Result presentation and discussion

OA was implemented with 15 agents ($I = 15$) and 75 iterations ($K = 75$), as outlined in the agent structure presented in Table 1. Besides, $\alpha = 0.7$, and $\beta = 0.3$. Stagnation around local optima is a significant issue

Table 2
Economic information of the Project.

Inflation rate (%)	Nominal rate (%)	Project lifetime (year)	Gasoline price (€/liter)	Target EIU (%)
2.5	4.25	25	1.6	1

affecting many modern optimization techniques, and the OA is no exception. To mitigate this, the OA was run 100 times using different seeds during random number generation. This approach enables the exploration of various local minima across the search space. The probability of discovering a new local minimum through additional OA runs was estimated using the method described in reference (Finch et al., 1989).

Fig. 4 illustrates the convergence of the OA across all 100 computational experiments. The different local minima reached are evident (the blue lines and the black one), with particular emphasis on the result that achieved the minimum NPC (the black line), which is presumed to be the global optimum.

Fig. 5 presents the NPC histogram of the configurations reached at the final iteration ($K = 75$) from the convergence shown in Fig. 4. This histogram provides valuable insight into the likelihood of identifying a new local optimum through repeated optimization. As observed, solutions near the minimum occurred more frequently due to the OA's search procedures. Based on the results shown in Fig. 5, the probability of discovering a previously unobserved local minimum by repeating the simulation was estimated to be 0.1065 in this case.

Figs. 6 and 7 analyze the performance of the configuration proposed by the OA in terms of normalized capacity and SOC. As indicated in Fig. 6, the estimated battery lifetime is 9.71 years. This lifespan is directly linked to the fact that the SOC is not expected to fall below 55 %, as illustrated in Fig. 7.

For comparison purposes, the HRES design was also optimized using a GA (Dufo-López and Bernal-Agustín, 2005), with a population size of 25 individuals, 50 generations, and crossover and mutation rates of 80 % and 10 %, respectively. GA is traditionally implemented in commercial programs without accounting for stagnation around a local optimum, a common issue associated with any MOA. Therefore, a comparative analysis was conducted by running GA a single time to evaluate the order of magnitude of NPC estimation obtained using OA with a typical GA implementation.

The corresponding results are presented in Table 3, which include the structure from Table 1. Given the abundant solar resources in Maiduguri, the OA recommended the PV panels with the highest power output and the maximum allowable number of strings, combined with a medium-sized wind turbine and LAB bank. In the case of the GA, a similar trend to that observed in the OA study can be identified: the significant integration of solar PV generation, complemented by moderate wind generation and LAB.

According to Table 4, the difference in NPC is found to be 0.45 %, with the GA result serving as the reference. In addition, Table 4 provides a comparison of the time taken by both methods. It is evident that the OA requires significantly more time than the GA. It is important to note that the OA was executed 100 times from different random starting points to gather information about the quality of the solution, reflected in the probability of discovering a new solution by repeating the optimization process, which in this case was 0.1065. Moreover, the OA evaluates the population more frequently than the GA. In contrast, the GA was run only once, with no specification or guarantee regarding the optimality of the solution obtained.

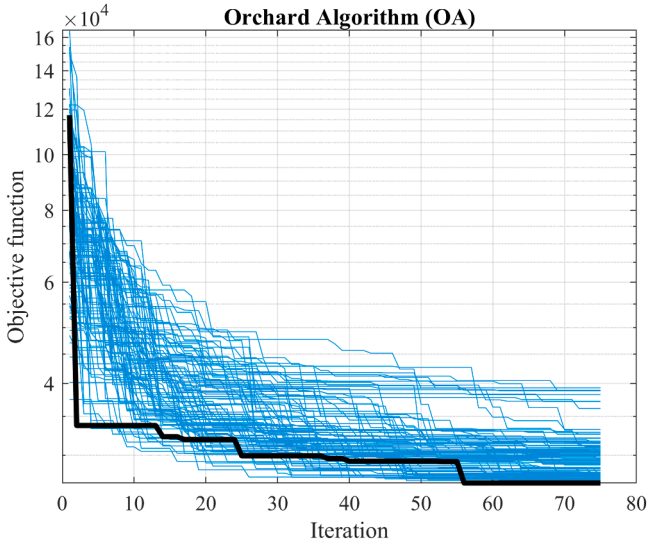

Fig. 4. Convergence process of the OA.

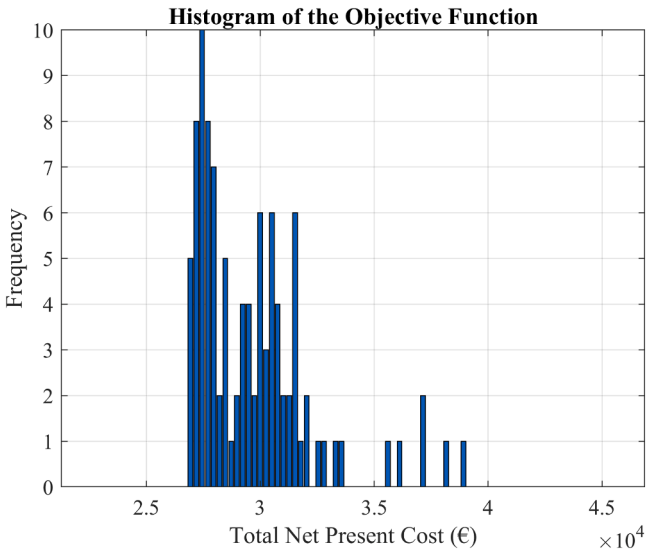

Fig. 5. Histogram of the NPC.

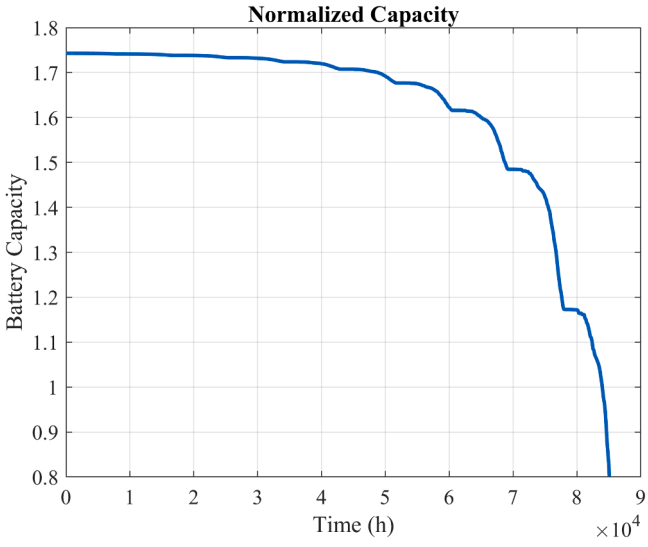

Fig. 6. LAB normalized capacity.

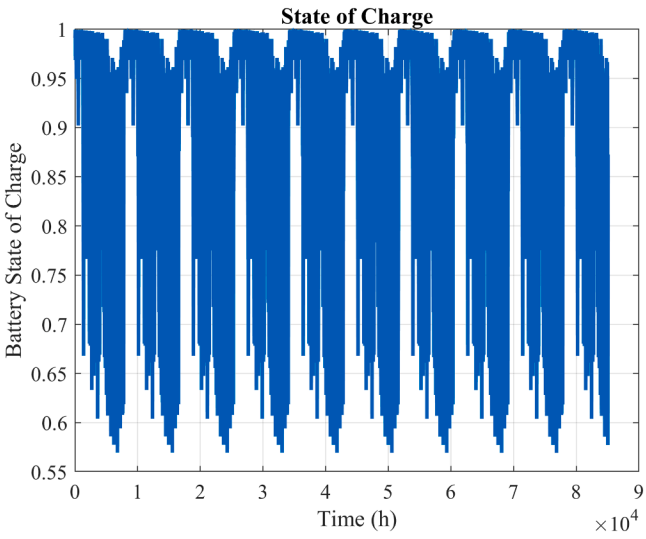

Fig. 7. LAB SOC.

5. Conclusions

This research proposed the use of the OA for the optimal sizing of an HRES for rural electrification. A hypothetical system in Maiduguri, Nigeria, was used to demonstrate the characteristics of the proposed approach. Specifically, the approach combines an HRES simulation model based on the weighted *Ah* throughput model with the search capabilities of the OA, achieving a balanced design from both technical and economic perspectives.

Global optimization is achieved by running the OA process 100 times with different seeds for random number generation, preventing stagnation at a local minimum. This methodology enables the exploration of multiple local minima and allows for the estimation of the probability of discovering a new one by repeating the optimization routine. It provides valuable insights into the optimality of the solution, which is essential for effective economic and resource management.

The obtained solution revealed that the economic benefit depends on integrating the abundant renewable resource—in this case, solar energy—complemented by a modest storage capacity. This approach allows for the efficient use of free and clean energy resources while minimizing high expenditures on energy storage devices.

Based on a comparative analysis with GA, it was observed that the operators utilized by the selected optimization method (OA or GA) influence both the identified local minimum and the likelihood of discovering additional ones through an extended optimization process. As the operators employed by OA are more advanced than those used by GA, the resulting histogram of the problem's solutions (Fig. 5) is more accurate. Consequently, the primary objective of using OA is to construct this histogram (Fig. 5) with high precision, thereby enabling the estimation of the probability associated with the identified local minimum. In other words, when multiple local minima are found, extending the optimization process allows for the estimation of the likelihood of uncovering an unobserved minimum. This, in turn, provides valuable insight into the extent to which a given local minimum may correspond to the global optimum. The operators within OA perform a comprehensive exploration and exploitation of the search space, enabling a precise characterization of the solution histogram (Fig. 5), the identification of promising local minima, and the probability that such a local minimum represents the global optimum.

In terms of cost, the solution obtained using OA is 0.45 % lower than that produced by a GA implementation. Throughout the optimization process, the search space was thoroughly explored, resulting in a probability of 0.1065 for identifying an additional local minimum. This probability is closely linked to the likelihood that the identified solution represents the global optimum. Such an analysis cannot be performed using commonly available commercial software (in this study, GA was used as a representative example), as these tools typically solve the optimization problem only once and do not provide further insights into the optimality of the solution. In addition to identifying competitive solutions in terms of NPC, it is also valuable to provide insight into the extent to which such a solution represents the global optimum.

CRediT authorship contribution statement

Eduardo García-Paricio: Visualization, Writing – review & editing, Writing – original draft, Methodology. **Rodolfo Dufo-López:** Funding acquisition, Supervision, Validation, Writing – original draft, Writing – review & editing, Formal analysis. **Jesús Sergio Artal-Sevil:** Writing – original draft, Resources, Data curation, Writing – review & editing, Investigation. **Lujano Rojas Juan Miguel:** Conceptualization, Project administration, Writing – review & editing, Writing – original draft, Software, Methodology.

Table 4
Economic performance of the optimal HRES.

Algorithm	Total net present cost (€)	Time (hh:mm:ss)
OA	26823.98	50:34:27
GA	26947.35	00:11:44

Table 3
Optimal HRES architecture.

Algorithm	Solar panel type (v)	Panels in parallel (d)	Wind turbine type (z)	Wind turbines (j)	Battery type (m)	Batteries in parallel (o)	Generator type (y)
OA	26 (600 W)	15	11 (2875 W)	1	17 (1879 Ah)	1	1 (0 W)
GA	25 (577 W)	13	12 (3150 W)	1	21 (2377 Ah)	1	1 (0 W)

Declaration of Generative AI and AI-assisted technologies in the writing process

During the preparation of this work the authors used ChatGPT-4o in order to improve the language and readability of the manuscript. After using this service, the author reviewed and edited the content as needed and take full responsibility for the content of the publication.

Funding

This work was supported by the Spanish Government (Ministerio de Ciencia e Innovación, Agencia Estatal de Investigación) and by the European Union / European Regional Development Fund [Grant PID2021-123172OB-I00 funded by MCIN/AEI/ 10.13039/501100011033 and by "ERDF A way of making Europe"]; [Grant TED2021–129801B-I00 funded by MCIN/AEI/ 10.13039/501100011033 and by European Union NextGenerationEU/PRTR].

Declaration of Competing Interest

The authors declare the following financial interests/personal relationships which may be considered as potential competing interests: Rodolfo Dufo-Lopez reports financial support was provided by Spanish Government (Ministerio de Ciencia e Innovación, Agencia Estatal de Investigación). Rodolfo Dufo-Lopez reports financial support was provided by European Regional Development Fund. If there are other authors, they declare that they have no known competing financial interests or personal relationships that could have appeared to influence the work reported in this paper.

Acknowledgment

This work was supported by the Spanish Government (Ministerio de Ciencia e Innovación, Agencia Estatal de Investigación) and by the European Union / European Regional Development Fund [Grant PID2021–123172OB-I00 funded by MCIN/AEI/ 10.13039/501100011033 and by "ERDF A way of making Europe"]; [Grant TED2021–129801B-I00 funded by MCIN/AEI/ 10.13039/501100011033 and by European Union NextGenerationEU/PRTR].

Data availability

The data is described in the manuscript and link are referenced

References

Ali, M.M., Mohammed, N., 2024. Optimal sizing of hybrid renewable energy systems using quasi-optimal control. Renew. Energy 226, 120351. https://doi.org/10.1016/j.renene.2024.120351.

Al-Odat, M., Al-Hasan, M., Obeidat, F., Chamkha, A.J., 2024. Optimization of on-grid hybrid PV/wind system for a cement factory in Kuwait using HOMER pro software. Int. J. Low. Carbon Technol. 19, 120–126. https://doi.org/10.1093/ijlct/ctad117.

Andersson, A., 2006. Battery lifetime modelling. Denmark National Laboratory Risø.

Bindner, H., Cronin, T., Lundsager, P., Manwell, J.F., Abdulwahid, U., Baring-Gould, I., 2005. Denmark National Laboratory Risø. Lifetime Model. Lead. Acid. Batter. ⟨https://www.osti.gov/etdeweb/servlets/purl/20607163⟩.

Y. Bourek, E.M.B. Messini, C. Ammari, M. Guenoune, B. Chabira, B.K. Saha, A hybrid renewable energy system for Hassi Messaoud region of Algeria: modeling and optimal sizing. Energy Storage and Saving In Press, (n.d.)https://doi.org/10.1016/j.enss.2024.10.002.

Coban, H.H., 2024. A multiscale approach to optimize off-grid hybrid renewable energy systems for sustainable rural electrification: economic evaluation and design. Energy Strategy Rev. 55, 101527. https://doi.org/10.1016/j.esr.2024.101527.

Dawsari, S.A., Anayi, F., Packianather, M., 2024. Techno-economic analysis of hybrid renewable energy systems for cost reduction and reliability improvement using dwarf mongoose optimization algorithm. Energy 313, 133653. https://doi.org/10.1016/j.energy.2024.133653.

Dufo-López, R., Bernal-Agustín, J.L., 2005. Design and control strategies of PV-Diesel systems using genetic algorithms. Sol. Energy 79, 33–46. https://doi.org/10.1016/j.solener.2004.10.004.

Finch, S.J., Mendell, N.R., Thode, H.C.J., 1989. Probabilistic measures of adequacy of a numerical search for a global maximum. J. Am. Stat. Assoc. 84, 1020–1023. ⟨https://www.jstor.org/stable/2290078⟩.

Huang, G.Q., Gan, J., Huang, Y., Ebrahimian, H., 2024. Optimization of off-grid renewable energy systems using a hybrid version of golden search algorithm. Heliyon 10, e30990. https://doi.org/10.1016/j.heliyon.2024.e30990.

Hussam, W.K., Barhoumi, E., Abdul-Niby, M., Sheard, G.J., 2024. Techno-economic analysis and optimization of hydrogen production from renewable hybrid energy systems: shagaya renewable power plant-Kuwait. Int. J. Hydrog. Energy 58, 56–68. https://doi.org/10.1016/j.ijhydene.2024.01.153.

Kaveh, M., Mesgari, M.S., Saeidian, B., 2023. Orchard algorithm: a new meta-heuristic algorithm for solving discrete and continuous optimization problems. Math. Comput. Simul. 208, 95–135. https://doi.org/10.1016/j.matcom.2022.12.027.

Khalid, W., Awais, Q., Jamil, M., Khan, A.A., 2024. Dynamic simulation and optimization of off-grid hybrid power systems for sustainable rural development. Electronics 13, 2487. https://doi.org/10.3390/electronics13132487.

Kohole, Y.W., Ngouleu, C.A.W., Fohagui, F.C.V., Tchuen, G., 2024. Optimization of an off-grid hybrid photovoltaic/wind/diesel/fuel cell system for residential applications power generation employing evolutionary algorithms. Renew. Energy 224, 120131. https://doi.org/10.1016/j.renene.2024.120131.

Lambert, T., Gilman, P., Lilienthal, P., 2006. Micropower system modeling with Homer. In: Farret, F.A., Godoy, S.M. (Eds.), Integration of alternative sources of energy. John Wiley & Sons, Inc, Hoboken, New Jersey, pp. 379–418.

Li, X., Tian, Z., Wu, X., Feng, W., Niu, J., 2024b. Optimal planning for hybrid renewable energy systems under limited information based on uncertainty quantification. Renew. Energy 237, 121866. https://doi.org/10.1016/j.renene.2024.121866.

Li, M.W., Yang, B., Duan, J.H., Shu, H.C., Wang, Y.T., Yang, Z.W., Jiang, L., Chen, Y.X., Sang, Y.Y., 2024a. Exponential slime mould algorithm based spatial arrays optimization of hybrid wind-wave-PV systems for power enhancement. Appl. Energy 373, 123905. https://doi.org/10.1016/j.apenergy.2024.123905.

Liu, X., Wang, J.-S., Zhang, S.-B., Guan, X.-Y., Gao, Y.-Z., 2024. Optimization scheduling of off-grid hybrid renewable energy systems based on dung beetle optimizer with convergence factor and mathematical spiral. Renew. Energy 237, 121874. https://doi.org/10.1016/j.renene.2024.121874.

Loh, B.-E.B., Nfah, E.M., 2024. Techno – economic and environmental design of a three – phase hybrid renewable energy system for UNVDA Ndop Cameroon using meta-heuristic and analytical approaches. Renew. Energy 237, 121527. https://doi.org/10.1016/j.renene.2024.121527.

Ma, X.M., Deveci, M., Yan, J., Liu, Y.Q., 2024. Optimal capacity configuration of wind-photovoltaic-storage hybrid system: a study based on multi-objective optimization and sparrow search algorithm. J. Energy Storage 85, 110983. https://doi.org/10.1016/j.est.2024.110983.

Menesy, A.S., Almomin, S., Sultan, H.M., Habiballah, I.O., Gulzar, M.M., Alqahtani, M., Khalid, M., 2024. Techno-economic optimization framework of renewable hybrid photovoltaic/wind turbine/fuel cell energy system using artificial rabbits algorithm. IET Renew. Power Gener. https://doi.org/10.1049/rpg2.12938.

Mohamed, M.A., Shadoul, M., Yousef, H., Al-Abri, R.R., Sultan, H.M., 2024. Multi-agent based optimal sizing of hybrid renewable energy systems and their significance in sustainable energy development. Energy Rep. 12, 4830–4853. https://doi.org/10.1016/j.egyr.2024.10.051.

Nduka, E., 2021. How to get rural households out of energy poverty in Nigeria: a contingent valuation. Energy Policy 149, 112072. https://doi.org/10.1016/j.enpol.2020.112072.

Ozturk, Z., Terkes, M., Demirci, A., 2024. Optimal planning of hybrid power systems under economic variables and different climatic regions: a case study of Türkiye. Renew. Energy 232, 121029. https://doi.org/10.1016/j.renene.2024.121029.

Pfenninger, S., Staffell, I., 2016. Long-term patterns of European PV output using 30 years of validated hourly reanalysis and satellite data. Energy 114, 1251–1265. https://doi.org/10.1016/j.energy.2016.08.060.

Prinsloo, G., Dobson, R., 2016. A. Brent, Scoping exercise to determine load profile archetype reference shapes for solar co-generation models in isolated off-grid rural African villages. J. Energy South. Afr. 27, 11–27. https://doi.org/10.17159/2413-3051/2016/v27i3a1375.

Rampinelli, G.A., Krenzinger, A., Romero, F.C., 2014. Mathematical models for efficiency of inverters used in grid connected photovoltaic systems. Renew. Sustain. Energy Rev. 34, 578–587. https://doi.org/10.1016/j.rser.2014.03.047.

Renewables.ninja. ⟨https://www.renewables.ninja/⟩ [accessed 15 October 2024].

Roshani, A.S., Assareh, E., Ershadi, A., Carvalho, M., 2024. Optimization of a hybrid renewable energy system for off-grid residential communities using numerical simulation, response surface methodology, and life cycle assessment. Renew. Energy 236, 121425. https://doi.org/10.1016/j.renene.2024.121425.

Roy, D., Zhu, S.M., Wang, R.Q., Mondal, P., Ling-Chin, J., Roskilly, A.P., 2024. Techno-economic and environmental analyses of hybrid renewable energy systems for a remote location employing machine learning models. Appl. Energy 361, 122884. https://doi.org/10.1016/j.apenergy.2024.122884.

Schiffer, J., Sauer, D.U., Bindner, H., Cronin, T., Lundsager, P., Kaiser, R., 2007. Model prediction for ranking lead-acid batteries according to expected lifetime in renewable energy systems and autonomous power-supply systems. J. Power Sources 168, 66–78. https://doi.org/10.1016/j.jpowsour.2006.11.092.

Staffell, I., Pfenninger, S., 2016. Using bias-corrected reanalysis to simulate current and future wind power output. Energy 114, 1224–1239. https://doi.org/10.1016/j.energy.2016.08.068.

Superchi, F., Moustakis, A., Pechlivanoglou, G., Bianchini, A., 2025. On the importance of degradation modeling for the robust design of hybrid energy systems including renewables and storage. Appl. Energy 377, 124645. https://doi.org/10.1016/j.apenergy.2024.124645.

Wang, Y., He, X., Liu, Q., Razmjooy, S., 2024. Economic and technical analysis of an HRES (Hybrid Renewable Energy System) comprising wind, PV, and fuel cells using an improved subtraction-average-based optimizer. Heliyon 10, e32712. https://doi.org/10.1016/j.heliyon.2024.e32712.

Yahya, W., Saied, K.M., Nassar, A., Qader, M.R., Al-Nehari, M., Zarabia, J., Jian, Z., 2024. Optimization of a hybrid renewable energy system consisting of a of PV/wind turbine/battery/fuel cell integration and component design. Int. J. Hydrog. Energy 94, 1406–1418. https://doi.org/10.1016/j.ijhydene.2024.11.187.

Yuan, T.M., Mu, Y., Wang, T., Liu, Z.M., Pirouzi, A., 2024. Using firefly algorithm to optimally size a hybrid renewable energy system constrained by battery degradation and considering uncertainties of power sources and loads. Heliyon 10, e26961. https://doi.org/10.1016/j.heliyon.2024.e26961.